Phonon wave effects in the thermal transport of epitaxial TiN/(Al,Sc)N metal/semiconductor superlattices

Bivas Saha, Yee Rui Koh, Joseph P. Feser, Sridhar Sadasivam, Timothy S. Fisher, Ali Shakouri, and Timothy D. Sands

Citation: Journal of Applied Physics **121**, 015109 (2017); doi: 10.1063/1.4973681
View online: http://dx.doi.org/10.1063/1.4973681
View Table of Contents: http://aip.scitation.org/toc/jap/121/1
Published by the American Institute of Physics

Phonon wave effects in the thermal transport of epitaxial TiN/(Al,Sc)N metal/semiconductor superlattices

Bivas Saha,[1] Yee Rui Koh,[2,3] Joseph P. Feser,[4] Sridhar Sadasivam,[5,3] Timothy S. Fisher,[5,3] Ali Shakouri,[2,3] and Timothy D. Sands[6]
[1]*Department of Materials Science and Engineering, University of California, Berkeley, California 94720, USA*
[2]*School of Electrical and Computer Engineering, Purdue University, West Lafayette, Indiana 47907, USA*
[3]*Birck Nanotechnology Center, Purdue University, West Lafayette, Indiana 47907, USA*
[4]*Department of Mechanical Engineering, University of Delaware, Newark, Delaware 19716, USA*
[5]*School of Mechanical Engineering, Purdue University, West Lafayette, Indiana 47907, USA*
[6]*Bradley Department of Electrical and Computer Engineering and Department of Materials Science and Engineering, Virginia Tech, Blacksburg, Virginia 24061, USA*

(Received 2 October 2016; accepted 22 December 2016; published online 6 January 2017)

Epitaxial single crystalline TiN/(Al,Sc)N metal/semiconductor superlattice metamaterials have generated significant interest in recent years for their potential applications in high temperature thermoelectric devices, optical hyperbolic metamaterials in the visible and near infrared-spectral range, and as candidates for solar-thermophotovoltaics and high temperature electronic materials. While significant progress in their structural, mechanical, and optical properties has been made, in-depth analysis and detailed understanding of their thermal transport mechanism remain to be addressed. In this article, we show that in short-period epitaxial, lattice-matched TiN/(Al,Sc)N metal/semiconductor superlattices, thermal transport is dominated by phonon wave effects as the wavelengths of phonons that carry significant amounts of heat become comparable to the superlattice period thickness. Due to the increasing contribution of such phonon wave-modes, the cross-plane thermal conductivity at short-periods increases with decreasing period thicknesses resulting in a distinct minimum of thermal conductivity at a period thickness of about 4 nm at room temperature. Thermal conductivity of the superlattices also decreases with an increase in the temperatures due to Umklapp scattering, which supports the wave-nature of the phonon transport mechanism. These results show that the lattice-matched, epitaxial TiN/(Al,Sc)N metal/semiconductor superlattices behave as an effective medium with respect to phonon transport at short-periods, and the wave-nature of phonon dominates the heat conduction mechanism at such length scales. *Published by AIP Publishing.* [http://dx.doi.org/10.1063/1.4973681]

I. INTRODUCTION

Ever since the theoretical proposal of Esaki[1,2] on the band-structure engineering of materials by employing artificially structured superlattices, semiconductor based superlattice metamaterials have impacted the world in many profound ways.[3,4] Semiconductor based superlattices such as GaAs/AlAs[5] and others have resulted in many novel physics based concepts and are actively researched and developed for many industrial applications. In contrast to the semiconductor/semiconductor superlattices, development of epitaxial, single-crystalline metal/semiconductor superlattices has eluded researchers for several decades primarily due to the extraordinarily difficult growth and material challenges.[6,7] Saha *et al.*[8–10] have recently developed the first epitaxial, single-crystalline, metal/semiconductor superlattices based on transition metal nitrides. The TiN/(Al,Sc)N metal/semiconductor superlattices are not just the first of its kind material system, they are amenable to doping, alloying, quantum size effects, and exhibit high mechanical hardness, chemical and thermal stability. The nitride superlattices have already established themselves as attractive plasmonic and nano-photonic materials as they exhibit hyperbolic dispersion of the iso-frequency surfaces,[9] and large enhancement of their photonic densities of states[11,12] has been demonstrated recently, which could be engineered for the next generation of quantum electronic and optoelectric device applications.

Understanding the principles and mechanism of heat transport in these novel superlattices is however extremely important not just for their intended thermoelectric and solar-thermophotovoltaic applications, but for almost all of their studies on fundamental transport physics and practical devices.[13–16] With a motivation to reduce the overall thermal conductivity necessary for thermoelectric devices, (Ti,W)N/(Al,Sc)N metal/semiconductor superlattices were recently developed as a sister material system[17] of the TiN/(Al,Sc)N metal/semiconductor superlattices, and it was demonstrated that the thermal conductivity reduces to as low as 1.7 W/m K at room temperature suitable for thermoelectricity. The study[17] also revealed that at short superlattice period thicknesses, the thermal conductivity saturates due to heavy alloy scattering of phonons from the tungsten (W) atomic sites, which eludes observation of any phonon wave effects in the (Ti,W)N/(Al,Sc)N superlattice system.

Observation of phonon wave-effects in superlattices however should be possible if the interface of the material is atomically clean and is devoid of any extended defects that destroy phonon wave interference. Moreover, observation of

phonon wave-effects in nitride superlattices could also open the possibility to engineer their thermal properties for many other applications such as hyperthermal conductivity and others.[18] As a general physics principle, the classical description of phonon transport in superlattices[13–16] treats the interfaces as a series of independent thermal resistances. As interface density is increased, the effective thermal conductivity of a superlattice is therefore predicted to decrease. However, as the period thickness becomes smaller, this classical treatment is expected to break down. For very short-periods, when the dominant phonon wavelengths involved in thermal transport become comparable to the period thickness, individual layers should lose their identity and the whole material could behave as an effective medium where phonon wave-modes propagate from one side to another without scattering from the interfaces. There have been recent efforts to investigate the wave-like thermal transport mechanisms[19–22] in superlattices. In this article, we show wave-like phonon transport in short-period epitaxial, lattice-matched TiN/$Al_{0.72}Sc_{0.28}N$ metal/semiconductor superlattices. These observations are important not just because it is the first experimental demonstration of the effect in a metal/semiconductor superlattice system, it would also add a lever to modify and engineer the heat conduction in nitride heterostructures.

II. METHODS

A. Growth

TiN/(Al,Sc)N thin film superlattices were grown on [001] MgO substrates with a reactive dc-magnetron sputtering technique inside a load-locked turbomolecular pumped high vacuum deposition system with a base pressure of 3–5 $\times$ 10^{-8} Torr (PVD Products, Inc.). The growth chamber had the capability to accommodate four targets and was equipped with three dc power supplies. The Sc (99.998% purity), Al (99.99%), and Ti (99.98%) targets had dimensions of 2 in. diameter and 0.25 in. thickness. All depositions were performed with an Ar/N_2 mixture having 6 sccm of N_2 and 4 sccm of Ar at a deposition pressure of 10 mTorr. The targets were sputtered in constant power mode. The substrates were maintained at 750 °C during deposition, as determined using an infrared pyrometer operated in the wavelength range of 0.8–1.1 μm, together with a thermocouple.

B. Time-domain thermoreflectance (TDTR) measurement

We employed time-domain thermoreflectance[23–25] (TDTR) to measure the thermal conductivity of the TiN/AlScN superlattice samples. TDTR is a nondestructive optical pump-probe method to measure thermal conductivity. A Ti: Sapphire laser was used in the TDTR setup to create short pulsed laser beams with ~12.5 ns repetition rate.[26,27] In the measurement, the laser pulses were split into pump beam and probe beam. The pump beam was used to create a temperature rise on the sample surface. In considering the thickness constraint of the samples (~240 nm), we modulated the pump beam at a frequency of 6–10 MHz. The pump modulation frequency (f) is inversely proportional to the heat penetration depth (d) with the relation of $d = \sqrt{\frac{k}{\Pi C_p f}}$, where k and C_p are the thermal conductivity and heat capacity of the film, respectively. The radii of the laser beam were in the range of 5.5–6.0 μm at the sample surface. A 100 nm TiN transducer was coated on the sample to absorb the incident beam. The probe laser is relatively low in laser power to probe the change of thermo-reflectance on the sample surfaces. A Si photodetector and RF lock-in amplifier was used to collect the reflected probe beam signal. The probe beam signal was fitted with a 3D thermal diffusion model based on thermal quadrupoles. The interface resistance between the TiN transducer and TiN/$Al_{0.72}Sc_{0.28}N$ was included in the model. In order to measure the thermal conductivity at different ambient temperatures, a Linkam THMS600 temperature stage was used. A temperature resolution of 0.1 °C was achieved.

III. RESULTS AND DISCUSSION

Metastable rocksalt $Al_{0.72}Sc_{0.28}N$ semiconductors (deposited by solid-state alloying of AlN with ScN) with the ability to lattice match to TiN have been previously described by our group (Ref. 8). For the current work, nominally monocrystalline rocksalt TiN/$Al_{0.72}Sc_{0.28}N$ metal/semiconductor superlattices were grown on [001] MgO substrates with 002 orientation (see Fig. 1(a)) and very low densities of extended defects. The full-width-at-half-maxima (FWHM) of the rocking curve (ω-scan) of these superlattices are in the 0.03°–0.10° range due to a small degree of mosaicity. X-ray reflectivity (XRR) analysis (not presented here, see Ref. 9) indicates that the interface roughness is of the order of one to two atomic layers for a superlattice having 10 nm period thickness. TEM and high-angle annular dark-field scanning transmission electron microscopy (HAADF-STEM) analyses (see Figs. 1(b) and 1(c)) confirm clear and distinct interfaces with the cube-on-cube epitaxial relationship of TiN(001)[100]|| MgO (001)[100] and $Al_{0.72}Sc_{0.28}N$ (001)[100]|| TiN (001)[100]. The superlattices are pseudomorphic with respect to the MgO substrates and they are stable at high temperatures (1050 °C for 4 h verified by synchrotron measurements, see Ref. 28). Time domain thermo-reflectance (TDTR) measurements were performed (as shown in the schematic in Fig. 2), using a capping layer of 100 nm TiN as the measurement transducer in-situ deposited on the superlattices. The total thickness of each superlattice was fixed at 240–250 nm, and the individual layers in the superlattices have thicknesses that are approximately half of the period thickness (see Fig. 3(a)). Thin-film samples of epitaxial TiN, $Al_{0.72}Sc_{0.28}N$, and $Ti_{0.5}(Al_{0.72}Sc_{0.28})_{0.5}N$ were also grown for independent thermal and electrical characterization. Details about the TDTR data fittings are presented in the supplementary material.

TDTR results indicate a room temperature cross-plane thermal conductivity for TiN of 63 W/m K (Fig. 3(b)). This is consistent with a previous report[29] for high-quality stoichiometric epitaxial TiN films. TiN is a dilute metal having a high carrier concentration (about 1–3 $\times$ 10^{21} per cc range) and a large electrical conductivity of 1.5 $\times$ 10^7 S/m at room temperature. Using the Wiedemann-Franz law to find and

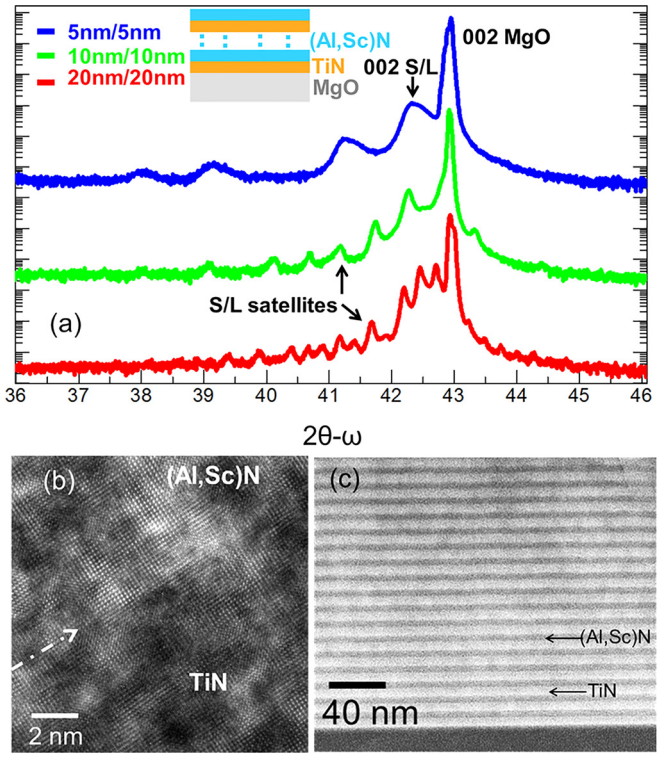

FIG. 1. (a) Symmetric 2θ-ω X-ray diffraction spectra of TiN/$Al_{0.72}Sc_{0.28}N$ superlattices having different period thicknesses. The superlattices grow with 002 orientations on 001 MgO substrates with a small degree of mosaicity. Clear and distinct satellite peaks are visible in the diffraction spectra that suggest sharp and abrupt superlattice interfaces. (b) High magnification transmission electron microscopy (HRTEM) image of a TiN/$Al_{0.72}Sc_{0.28}N$ interface that shows cube-on-cube epitaxial crystal growth. (c) A representative high-angle annular dark-field scanning transmission electron microscopy (HAADF-STEM) image that shows uniform TiN (8 nm thick) and $Al_{0.72}Sc_{0.28}N$ (6 nm thick) layers separated by sharp interfaces. The total thickness of the superlattices employed in this study is kept constant at 240–250 nm, and individual layers in the superlattices have a thickness that is half of its period thickness.

subtract the electronic contribution gives an estimate of the phonon contribution to the TiN thermal conductivity of 17 W/m K. Fig. 3(b) also indicates that at room temperature, the semiconducting $Al_{0.72}Sc_{0.28}N$ film has a thermal

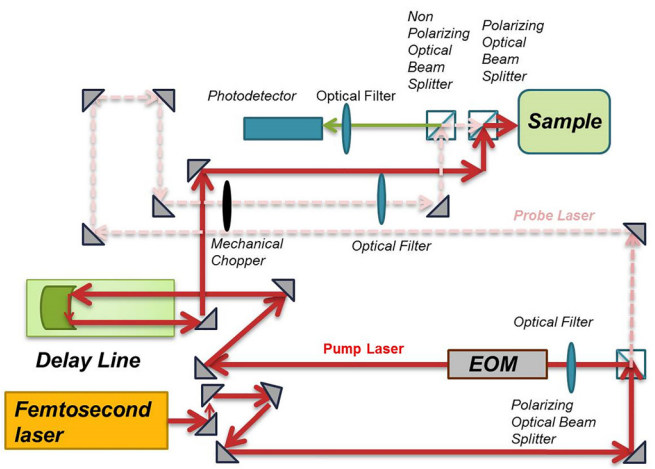

FIG. 2. Schematic of the time-domain thermoreflectance (TDTR) measurement system. The pump and probe beams are represented by solid and dashed lines, respectively.

conductivity of 4.5 W/m K. Since $Al_{0.72}Sc_{0.28}N$ is a metastable rocksalt semiconducting alloy with high electrical resistivity (see Ref. 8), the thermal conductivity is dominated by its phonon contribution.

The cross-plane thermal conductivity measurements of the superlattices as a function of period thickness show a minimum at a period thickness of about 4 nm at room temperature (see Fig. 3(b)). When the period thicknesses of the superlattices are large (e.g., 240 nm for a 120 nm TiN/120 nm $Al_{0.72}Sc_{0.28}N$ one period superlattice (or a bilayer)), the measured thermal conductivity is high (9.6 W/m K), but consistent with the series conductance of the individual layers. However, as the interface density is increased by reducing the period thickness, the thermal conductivity decreases due to the increased role of thermal interface resistance. For a 2 nm TiN/2 nm $Al_{0.72}Sc_{0.28}N$ superlattice, the TDTR measurements yield a thermal conductivity of 4.5 W/m K at room temperature. With the reduction of the period thickness from 240 nm to 4 nm, the thermal conductivity therefore decreases by a factor of 2.2×. We contend that above 4 nm period thicknesses, phonon transport in TiN/$Al_{0.72}Sc_{0.28}N$ superlattices is primarily (classical) particle-like with an interface-dominant incoherent scattering transport mechanism.

The decrease in the period thicknesses below 4 nm increases the cross-plane thermal conductivity (see Fig. 3(b)). We find that with a decrease in the period thicknesses from 4 nm to 0.8 nm, the thermal conductivity increases by a factor of 2.1× at room temperature. As will be discussed in detail, no structural changes have been observed, which would explain this behavior. It is clear that no phonon transport model that neglects the wave nature of phonons can explain such an increase in the thermal conductivity, so it is postulated that the role of coherent phonon effects may play a role in the thermal transport process. The dominant phonon modes that contribute to the thermal transport for short-periods have wavelengths on the order of a few nanometers and therefore may only see an effective medium when the superlattice period thickness is this short. Under the above description therefore we see a minimum when the period thickness is comparable to the wavelength of the phonons that both carry a significant amount of heat and are not strongly scattered by the interfaces.

To gain additional insight into the thermal transport mechanisms, the cross-plane thermal conductivity of each of the individual superlattices was measured at 150 K and 500 K, respectively (Fig. 3(c)). Results show two distinct transport regimes at low and high superlattice periods. The nature of the thermal conductivity curve at 150 K is very similar to that which we have measured at room temperature. However, at 500 K, thermal conductivity values are significantly lower due to high-temperature anharmonic (Umklapp) scattering.

To understand the wave-nature of thermal conduction, more refined temperature dependent thermal conductivity measurements were performed for a few samples, choosing two superlattices each from two distinct transport regimes and one sample near the minimum thermal conductivity at room temperature. Results given in Fig. 3(d) show that high

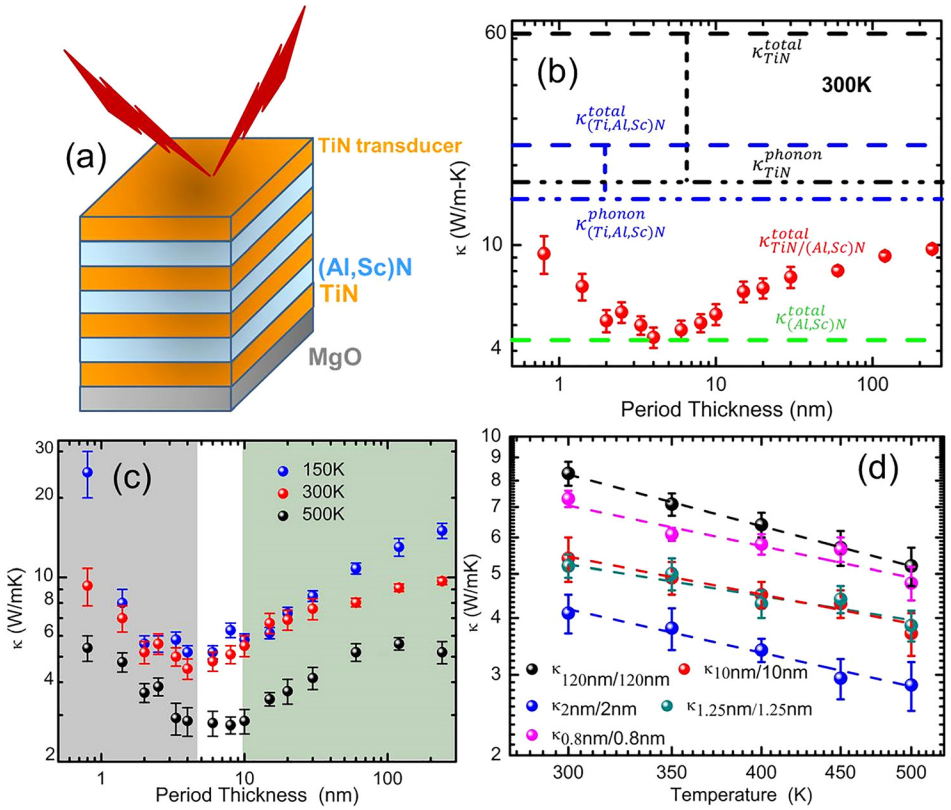

FIG. 3. (a) Schematic of TiN/$Al_{0.72}Sc_{0.28}N$ metal/semiconductor superlattices grown on the MgO substrate having TiN as a transducer layer on top. (b) Cross-plane thermal conductivity of TiN/$Al_{0.72}Sc_{0.28}N$ superlattices is presented as a function of period thickness at room temperature. Thermal conductivities of TiN, $Al_{0.72}Sc_{0.28}N$, and $Ti_{0.5}Al_{0.36}Sc_{0.14}N$ thin films at room temperature are also presented as lines on the same plot. Superlattice thermal conductivity shows a distinct minimum at 4 nm period thicknesses. (c) Cross-plane thermal conductivity of the superlattices at 150 K, 300 K, and 500 K, respectively, which shows that the minima in thermal conductivity as a function of period thickness persist even at different temperatures. (d) Temperature dependent cross-plane thermal conductivity of five different superlattices that span different phonon transport regimes. At higher temperatures, the thermal conductivity of the superlattices decreases due to Umklapp scattering.

temperature thermal transport in TiN/$Al_{0.72}Sc_{0.28}N$ superlattices is highly temperature dependent, indicating that Umklapp scattering is important. Note that conventional phonon thermal interface conductance models all predict interface conductance that increases with temperature;[30] therefore, the observed dependence is the opposite of what would be expected for interface limited phonon transport, albeit with different values of the scattering exponents (α) in $\kappa = AT^{\alpha}$ (see Table I). For large period thicknesses, when the individual materials are bulk-like (e.g., the 120 nm TiN/120 nm $Al_{0.72}Sc_{0.28}N$ sample), the exponent is −0.92. However, as the period thicknesses are reduced, the Umklapp scattering exponent decreases to smaller values such as −0.66 for the superlattice having 1.6 nm period thickness (see Table I for details).

The effect of atomic intermixing at the interfaces on the cross-plane thermal conductivity has been investigated. As noted previously,[9] XRR indicates a chemical roughness of 1–2 atomic layers, although the characteristic horizontal length-scale of that roughness cannot be established by XRR. When $Al_{0.72}Sc_{0.28}N$ layers grow on TiN, the interface roughness was measured to be ∼0.2 nm (∼1 atomic layer); while in the interfaces where TiN is deposited on $Al_{0.72}Sc_{0.28}N$ layers, the XRR shows a roughness of ∼0.4 nm (∼2 atomic layers). In addition, HRTEM and HAADF-STEM images have been obtained on superlattice samples (adapted from our previous publication[11] and presented in the supplementary material) that clearly show distinct and clear 2 nm $Al_{0.72}Sc_{0.28}N$ layers sandwiched between 20 nm TiN layers. Also, careful observation of the thermal conductivity data shows that the superlattice with 0.8 nm period thickness (thinnest in the present study) has a room temperature thermal conductivity of 9.2 W/m K, while the $Ti_{0.5}Al_{0.36}Sc_{0.14}N$ alloy has a room temperature thermal conductivity of 23 W/m K; therefore, even in the most extreme case, superlattices do not behave as a random alloy and intermixing is not likely to be the dominant effect.

TABLE I. Umklapp scattering exponent (α) of TiN/$Al_{0.72}Sc_{0.28}N$ superlattices as a function of period thickness.

Period thickness (nm)	α in $\kappa = AT^{\alpha}$
240	−0.91 ± 0.03
20	−0.71 ± 0.14
4	−0.76 ± 0.08
2.5	−0.55 ± 0.10
1.6	−0.66 ± 0.09

As mentioned earlier, there have been some recent efforts to understand the effect of phonon wave-effects in superlattices experimentally.[19,20] For example, Ravichandran *et al.*[20] has observed a similar increase in the cross-plane thermal conductivity in short-period $SrTiO_3/CaTiO_3$ and $SrTiO_3/BaTiO_3$ superlattices, which he has attributed to incoherent-to-coherent regime transition. While their pioneering work is one of the early demonstrations of coherent phonon heat transport in superlattices, careful observations however show that the thermal conductivity increased by a factor of 1.1× for the $SrTiO_3/CaTiO_3$ system at short periods, and no clear well defined increase of thermal conductivity at short periods was observed in the case of the $SrTiO_3/BaTiO_3$ superlattices. In contrast, the TiN/$Al_{0.72}Sc_{0.28}N$ superlattices show clear and distinct 2.1× increases in the thermal conductivity with a pronounced minimum at 4 nm period thicknesses at room temperature, which mark a progress in the quest to observe phonon wave effects in superlattices. At 150 K and 500 K,

the increase in the thermal conductivity with respect to their minima is also found to be a factor of 5× and 1.83×, respectively, for the $TiN/Al_{0.72}Sc_{0.28}N$ superlattices, which supports the wave-nature of phonon transport in these short-period superlattices. We note that Ravichandran *et al.*[20] also has reported 2× and 1.5× increase in the thermal conductivity at 84 K and 142 K, respectively, with respect to the minimum values for the $SrTiO_3/CaTiO_3$ short-period superlattices.

Although our results clearly show two different phonon transport regimes with respect to the periodicity of the $TiN/Al_{0.72}Sc_{0.28}N$ superlattices, we also note that such a transition is not abrupt. Phonon transport in superlattices (as in normal bulk materials) is a broadband phenomenon with different phonon modes having their own transport and scattering mechanisms. In the case of a thick $TiN/Al_{0.72}Sc_{0.28}N$ bilayer (e.g., 240 nm period thickness), even though a significant portion of the phonons undergo incoherent boundary scattering at the interfaces, there should still be some long-wavelength phonon modes that propagate from one side to the other without any scattering from the interfaces. Therefore, to identify such long wavelength phonon modes and to quantify their relative contributions to the overall thermal transport in superlattices, we analyze the interface thermal conductance (*ITC*) and compare the *ITC's* of superlattices having different period thicknesses. Equating total thermal resistance of a superlattice with the sum of resistances of the individual layers and the interface thermal resistance, we find

$$\frac{1}{\kappa_{superlattice}} = \frac{1}{2}\left(\frac{1}{\kappa_{TiN}} + \frac{1}{\kappa_{(Al,Sc)N}}\right) + \left(\frac{1}{GL}\right)N, \qquad (1)$$

where N, G, and L are the number of interfaces, the *ITC* of one interface, and the total thickness of the superlattice, respectively, while $\kappa_{superlattice}$, κ_{TiN}, $\kappa_{(Al,Sc)N}$ are the thermal conductivities of the superlattice, TiN, and (Al,Sc)N layers, respectively. To estimate the *ITC* from Eq. (1), knowledge of the thermal conductivity of individual layers within the superlattices is required. However, individual layer thicknesses are too small to allow direct measurement by our experimental method. Therefore, we plot $\frac{1}{\kappa_{superlattice}}$ as a function of N (see Fig. 4(a)), and use the slope to calculate the *ITC* in different period thickness regimes. Fig. 4(a) suggests three distinct regimes where a linear fit can be made to calculate the *ITC*. When the period thickness is large and the numbers of interfaces are small, data fitting of Fig. 4(a) suggests that the *ITC* at room temperature is 2.4 GW/m^2 K. This is an extremely high interface conductance for a metal-semiconductor interface, nearly 3× higher than the highest known metal-insulator interface,[29] TiN/MgO. On the other hand, when the period thickness is very small and the number of interfaces is large, the *ITC* is 11.9 GW/m^2 K (note, we have only used superlattices having period thicknesses larger than or equal to 4 nm for the *ITC* estimates). In the intermediate period thickness range, the *ITC* is about 7.6 GW/m^2 K at room temperature. Therefore, the results show that as the period thickness of the superlattice is reduced, the *ITC* increases significantly. Compared to the large period thickness regime, the short-period superlattices have 5× times larger *ITC* at room temperature. Such enhancement of *ITC* with decreasing period thickness[31] is intricately related to the increasing contribution of phonon modes with wavelengths longer than the period thickness in the overall thermal transport of these superlattices. Since the minimum wavelength of a phonon mode that does not see an interface and travels ballistically from one side to the other of a superlattice is comparable to the superlattice period thickness, a decrease in the period thickness allows increasing numbers of such phonon modes to participate in conduction without any incoherent scattering from the interfaces. With increasing numbers of these long-wavelength phonon modes, the interface thermal conductance therefore also increases with decreasing period thickness.[32] Our results are therefore in agreement with the physical picture of Luckyanova *et al.*,[19] which suggests that for a ~206 nm thick GaAs/AlAs superlattice with a period thickness of 14 nm, 86% of total thermal transport in superlattices involves contributions from long-wavelength phonon modes. The ITC at 150 K and 500 K is also extracted from the experimental results of Fig. 3(c) following the same procedure as that employed in Fig. 4(a) and plotted in Fig. 4(b) for the larger period superlattices. We find that the ITC extracted from larger period superlattices is 2 GW/m^2 K and 1.3 GW/m^2 K at 150 K and 500 K, respectively. Therefore, we see that the ITC at 150 K is very similar to that at 300 K, while the ITC at 500 K is about 2× smaller than that estimated at 300 K.

Comparison of *ITCs* estimated from experimental results with those of the standard interface transport models like acoustic mismatch model (AMM)[13] and diffuse mismatch model (DMM) with the Debye approximation[13] as well as full Brillouin zone dispersions[30] provides important insights into the thermal transport mechanism of superlattices. To obtain the Debye temperature, phonon group velocities and phonon frequencies over the entire Brillouin zone are necessary. We have performed first-principles density functional perturbation theory (DFPT) based calculations of the vibrational spectra of TiN and (Al,Sc)N. A detailed discussion of the calculation methodology and the analysis of their dispersion spectra are presented in the supplementary material. In Fig. 4(b), we present the calculated *ITCs* as a function of temperatures with the experimentally measured *ITC* for the largest period (240 nm period thickness) superlattice (which is essentially a bilayer) at room temperature. Since the interface transport models used here are valid strictly for bulk single hetero-interfaces with the component materials having large thicknesses,[13] comparison of the *ITC* values should only be made with our thick-period bilayer. Fig. 4(b) shows that the DMM calculation predicts an *ITC* of 0.6 GW/m^2 K at room temperature. AMM calculations that are expected to work best for lattice-matched coherent interfaces predict that the *ITC* at room temperature is 0.9 GW/m^2 K, which is very close to the radiation approximation (calculated by using Debye dispersion) representing the upper limit of the *ITC*. Therefore, the experimental measurements of the *ITC*s at room temperature are about 3× times larger than that of the radiation limit. Most of the practical interface theoretical models overestimate the *ITC* values, since these models

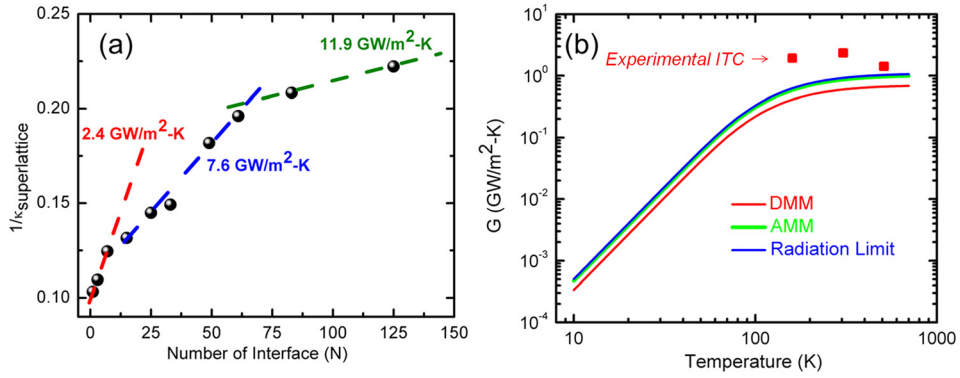

FIG. 4. (a) $(\frac{1}{\kappa_{superlattice}})$ is plotted as a function of the number of interfaces in superlattices to estimate the interface thermal conductances (ITCs) at room temperature. Three different transport regimes are observed in the figure; for very large period superlattices, the ITC is found to be 2.4 GW/m^2 K, while for very short-period superlattices the ITC is estimated to be 11.9 GW/m^2 K. (b) Modeling analysis of the interface thermal conductance (ITC) is presented as a function of temperatures. The acoustic mismatch model (AMM) and diffuse mismatch model (DMM) with Debye approximations are used to calculate the ITCs. Since the theoretical models assume infinitely thick layers in each side of the interfaces for the ITC calculations, experimental ITC values from the thickest period TiN/(Al,Sc)N superlattices are added in the figure for the comparison of results.

assume perfect interfaces, whereas real material interfaces always have some inhomogeneity and defects that scatter phonons and reduce the *ITC*. Although in an indirect way, these analyses therefore suggest that as the period thickness is decreased, the wave-nature of phonon modes becomes increasingly dominant. This wave-like nature of phonon transport cannot be captured in any conventional theoretical *ITC* models, as *ITCs* as a concept were not intended to be used in the regime where phonons with wavelengths longer than the period thickness contribute significantly to heat conduction.

While the experimental results and modeling analyses confirm the existence of wave-like nature of phonon transport and indicate their dominant nature in the heat conduction of short-period superlattices, the presence of TiN as the metallic component material warrants that we address the electronic contribution to the total thermal conductivity along the cross-plane direction of the superlattices, and more specifically the question of electronic tunneling current in short-period superlattices. Cross-plane electrical measurements of a 10 nm TiN/10 nm $Al_{0.72}Sc_{0.28}N$ superlattice were performed and the results suggest a room temperature electrical conductivity of 1.1×10^3 S/m. Assuming the applicability of the Wiedemann-Franz's law, we find that the electronic contribution to the total cross-plane thermal conductivity of this specific superlattice is less than 1% of its total value. Such small cross-plane electrical conductivity is presumably due to the large Schottky barrier height across the TiN/$Al_{0.72}Sc_{0.28}N$ interface. Therefore, the electronic contributions to the total thermal conductivity can be safely neglected for thicker superlattices. For very thin period superlattices, however, there could be an appreciable tunneling current across the interface. Measurement of such cross-plane tunneling electrical currents in short-period superlattices is extremely challenging, and we do not have an estimate of the tunneling current in these materials. However based on the available thermal conductivity results, we can conclude certain details about the tunneling current. It is known very well[33] that Fermi-level tunneling is independent of temperature, however we see from Fig. 3(a) that with the increase in temperature from 150 K to 500 K, the thermal conductivity decreases by about 2× on average in all short-period superlattices. Such a large decrease in thermal conductivity cannot be due to electronic tunneling current across the interface. In the case of thermionic-field emission, the electronic current would increase with temperature for the smallest period superlattices. The experimental results indicate the opposite behavior. Tunneling electrical current therefore cannot explain the thermal transport characteristics of short-period superlattices.

IV. CONCLUSION

In conclusion, we demonstrate wave-like thermal transport in short-period epitaxial, nominally monocrystalline TiN/$Al_{0.72}Sc_{0.28}N$ metal/semiconductor superlattices. Our results show a clear minimum (at 4 nm period thickness) in the cross-plane thermal conductivity as a function of the period thicknesses. At short-period thicknesses (less than 4 nm), the thermal conductivity increases with decreasing period thickness as the phonon modes that do not scatter from the interface contribute significantly to the thermal transport. Temperature dependent thermal conductivity measurements also support the wave-nature of thermal transport. We have addressed fundamental questions in the heat transport of nanoscale metal/semiconductor superlattices that have the potential to help in designing the next generation of efficient thermoelectric devices and thermal management technologies.

SUPPLEMENTARY MATERIAL

See supplementary material for details of first-principles density functional perturbation theory calculation, vibrational spectra of TiN and (Al, Sc)N, Interface Thermal Conductance (ITC) modeling: AMM, DMM and full Brillouin zone DMM, Interface Thermal Conductance (ITC) estimates, HRTEM and HAADF-STEM images, assumptions about the heat capacities of the materials vs. temperature, plot of the TiN/superlattice interface conductance versus period thickness and temperature, discussion on the sensitivities of the ratio data to the

thermal conductivity of the sample, discussion on assumptions about the sample/MgO interface conductance, temperature dependence of the alloy thermal conductivities, and compositions and thickness measurement.

ACKNOWLEDGMENTS

B.S. and S.S. thank Professor Supriyo Dutta and Professor David Cahill for helpful discussions. B.S. thanks Dr. Magnus Garbrecht and Dr. Jeremy Schroeder for assisting with microscopy analysis. B.S. and T.D.S. acknowledge financial support from the National Science Foundation and U.S. Department of Energy (CBET-1048616). Y.K. and A.S. acknowledge financial support from DARPA/Army Research Office, Contract No. W911NF0810347. S.S. and T.F. acknowledge financial support from the Office of Naval Research (Award No.: N000141211006).

The authors declare no competing financial interest.

[1]R. Tsu and L. Esaki, Appl. Phys. Lett. **22**, 562–564 (1973).
[2]L. Esaki and L. L. Chang, Phys. Rev. Lett. **33**, 495 (1974).
[3]K. Esaki, "A bird's-eye view on the evolution of semiconductor superlattices and quantum wells," in *Electronic Structure of Semiconductor Heterojunctions* (Springer, Netherlands, 1988), pp. 56–69.
[4]L. Esaki and R. Tsu, IBM J. Res. Dev. **14**, 61–65 (1970).
[5]A. Sibille, J. F. Palmier, H. Wang, and F. Mollot, Phys. Rev. Lett. **64**, 52 (1990).
[6]B. Saha, A. Shakouri, and T. D. Sands, "Metal/semiconductor superlattices: Development of an elusive heterostructure" (unpublished).
[7]K. N. Tu, IBM J. Res. Dev. **34**, 868 (1990).
[8]B. Saha, S. Saber, G. V. Naik, A. Boltasseva, E. Stach, E. P. Kvam, and T. D. Sands, Phys. Status Solidi B **252**(2), 251–259 (2015).
[9]B. Saha, G. V. Naik, S. Saber, E. Stach, V. M. Shalaev, A. Boltasseva, and T. D. Sands, Phys. Rev. B **90**, 125420 (2014).
[10]B. Saha, S. K. Lawrence, J. L. Schroeder, J. Birch, D. F. Bahr, and T. D. Sands, Appl. Phys. Lett. **105**, 151904 (2014).
[11]G. V. Naik, B. Saha, J. Liu, S. M. Saber, E. Stach, J. M. K. Irudayaraj, T. D. Sands, V. M. Shalaev, and A. Boltasseva, Proc. Natl. Acad. Sci. U.S.A. **111**, 7546 (2014).
[12]M. Y. Shalaginov, V. V. Vorobyov, J. Liu, M. Ferrera, A. V. Akimov, A. Lagutchev, A. N. Smolyaninov, V. V. Klimov, J. Irudayaraj, A. V. Kildishev, A. Boltasseva, and V. M. Shalaev, Laser Photonics Rev. **9**(1), 120–127 (2015).
[13]E. T. Swartz and R. O. Pohl, Rev. Mod. Phys. **61**, 605 (1989).
[14]D. G. Cahill, W. K. Ford, K. E. Goodson, G. D. Mahan, A. Majumdar, H. J. Maris, R. Merlin, and S. R. Phillpot, J. Appl. Phys. **93**, 793–818 (2003).
[15]S. M. Lee, D. G. Cahill, and R. Venkatasubramanian, Appl. Phys. Lett. **70**, 2957 (1997).
[16]G. Chen and M. Neagu, Appl. Phys. Lett. **71**(19), 2761 (1997).
[17]B. Saha, Y. R. Koh, J. Comparan, S. Sadasivam, J. L. Schroeder, M. Garbrecht, J. Birch, T. S. Fisher, A. Shakouri, and T. D. Sands, Phys. Rev. B **93**, 045311 (2016).
[18]J. Liu and E. Narimanov, Phys. Rev. B **91**, 041403 (2015).
[19]M. N. Luckyanova, J. Garg, K. Esfarjani, A. Jandl, M. T. Bulsara, A. J. Schmidt, A. J. Minnich, S. Chen, M. S. Dresselhaus, Z. Ren, E. Fitzgerald, and G. Chen, Science **338**, 936–939 (2012).
[20]J. Ravichandran, A. K. Yadav, R. Cheaito, P. B. Rossen, A. Soukiassian, S. J. Suresha, J. C. Duda., B. M. Foley, C. Lee, Y. Zhu, A. W. Lichternberger, J. E. Moore, D. A. Muller, D. G. Schlom, P. E. Hopkins, A. Majumdar, R. Ramesh, and M. Zurbuchen, Nat. Mater. **13**, 168–172 (2014).
[21]Z. Tian, K. Esfarjani, and G. Chen, Phys. Rev. B **89**, 235307 (2014).
[22]N. K. Ravichandran and A. Minnich, Phys. Rev. B **89**, 205432 (2014).
[23]D. G. Cahill, Rev. Sci. Instrum. **75**, 5119 (2004).
[24]S. Dilhaire, G. Pernot, G. Calbris, J. M. Rampnoux, and S. Grauby, J. Appl. Phys. **110**, 114314 (2011).
[25]A. J. Schmidt, X. Chen, and G. Chen, Rev. Sci. Instrum. **79**, 114902 (2008).
[26]B. Vermeersch, G. Pernot, Y. Koh, P. Abumov, and A. Shakouri, in *Proceedings of the 13th InterSociety Conference on Thermal and Thermomechanical Phenomena in Electronic Systems (ITherm)*, 2012, pp. 428–434.
[27]L. E. Cassels, T. E. Buehl, P. G. Burke, C. J. Palmstrøm, A. C. Gossard, G. Pernot, A. Shakouri, C. R. Haughn, M. F. Doty, and J. M. O. Zide, J. Vac. Sci. Technol., B **29**, 03C114 (2011).
[28]J. L. Schroeder, B. Saha, M. Garbrecht, N. Schell, T. D. Sands, and J. Birch, J. Mater. Sci. **50**(8), 3200–3206 (2015).
[29]R. M. Costescu, M. A. Wall, and D. G. Cahill, Phys. Rev. B **67**, 054302 (2003).
[30]P. Reddy, K. Castelino, and A. Majumdar, Appl. Phys. Lett. **87**, 211908 (2005).
[31]M. V. Simkin and G. D. Mahan, Phys. Rev. Lett. **84**, 927 (2000).
[32]A. S. Henry and G. Chen, J. Comput. Theor. Nanosci. **5**, 141 (2008).
[33]R. Hrach, Czech. J. Phys. B **18**, 402 (1968).